A three-dimensional silicon photonic crystal nanocavity with enhanced emission from embedded germanium islands

2012 New J. Phys. 14 083035

(http://iopscience.iop.org/1367-2630/14/8/083035)

New Journal of Physics
The open-access journal for physics

A three-dimensional silicon photonic crystal nanocavity with enhanced emission from embedded germanium islands

N Hauke[1,2,5], A Tandaechanurat[1,5], T Zabel[2], T Reichert[2], H Takagi[1], M Kaniber[2], S Iwamoto[1], D Bougeard[2,3], J J Finley[2,6], G Abstreiter[2,4,6] and Y Arakawa[1,4,6]

[1] Institute of Industrial Science, Institute for Nano Quantum Information Electronics, The University of Tokyo, 4-6-1 Komaba, Meguro, Tokyo 153-8505, Japan
[2] Walter Schottky Institut and Physik Department, Technische Universität München, Am Coulombwall 4, D-85748 Garching, Germany
[3] Institut für Experimentelle und Angewandte Physik, Universität Regensburg, D-93040 Regensburg, Germany
[4] Institute for Advanced Study, Technische Universität München, D-85748 Garching, Germany
E-mail: finley@wsi.tum.de, abstreiter@wsi.tum.de and arakawa@iis.u.tokyo.ac.jp

New Journal of Physics **14** (2012) 083035 (11pp)
Received 19 June 2012
Published 29 August 2012
Online at http://www.njp.org/
doi:10.1088/1367-2630/14/8/083035

Abstract. We report the realization of a silicon three-dimensional photonic crystal nanocavity containing self-assembled germanium-island emitters. The three-dimensional woodpile photonic crystal was assembled layer by layer by micromanipulation using silicon plates grown by molecular beam epitaxy. An optical nanocavity was formed in the center of the photonic crystal by introducing a point defect into one of the plates. Measurements of the filtered spontaneous emission from the Ge islands in the active plate through the localized modes of the structure directly reveal information on the evolution

[5] These authors contributed equally to this work.
[6] Authors to whom any correspondence should be addressed.

of the frequency and Q-factor as upper cladding plates are sequentially added. An exponential increase of the cavity-Q is observed when the number of upper cladding plates is increased up to a maximum of ten. The emission of germanium-islands within the cavity reveals several strongly polarized cavity modes with quality-factors up to ≈13 600. The emission intensity of the cavity modes is enhanced by large factors up to ≈ 58× as compared with the active plate outside the photonic environment.

Integrated silicon (Si)-based photonic circuits are of great interest since they would allow for the realization of high-speed optical interconnects that are fully compatible with standard CMOS technologies [1, 2]. A vital component of such interconnects is an efficient Si-based light source to interconvert between electrical and optical signals. However, crystalline Si is not suitable due to the very low internal quantum efficiency arising from its indirect band gap. In recent years, the use of cavity quantum electrodynamics phenomena in nanocavities has opened up the way for enhancing the intrinsic quantum efficiency; an impressive emission enhancement has been reported for two-dimensional (2D) crystalline Si photonic crystals (PhCs) [3–5] as well as for active emitters such as self-assembled germanium-islands (Ge islands) [6–11], embedded in a Si 2D PhC nanocavity. However, their inherent two-dimensionality limits the versatility for photonic applications, such as the design of a photonic network with directed routing of radiation while maintaining high cavity finesse. In sharp contrast, 3D Si PhCs offer much stronger potential for integrated photonic circuits due to their omnidirectional photonic band gap [12, 13]. Hence, over the last few years, much effort has been invested into the development of 3D PhCs using silicon [14–16]. In recent years, point defect resonators have been introduced and probed via reflection and transmission spectroscopy [17, 18]. However, all realizations of 3D PhC nanocavities using silicon to date were passive; that is, they did not contain embedded emitters.

In this paper, we demonstrate an *active*, high-quality Si 3D PhC nanocavity, which contains Ge islands as internal light emitters. Woodpile 3D PhCs [19, 20] are fabricated using molecular beam epitaxy (MBE) grown *passive* Si plates that are lithographically patterned and assembled using micromanipulation [21–24]. The Ge islands, embedded in a single *active* plate into which a defect nanocavity is formed, radiatively couple to the cavity modes allowing us to directly probe them by detecting the emitted photoluminescence (PL). The results show several strongly polarized cavity modes with quality-factors up to ≈13 600 and an emission intensity that is enhanced by factors up to ≈ 60× compared with the same material outside the photonic environment.

The passive and active plates were fabricated from a commercial silicon-on-insulator (SOI) wafer with a nominally 220 nm thick Si device layer on top of 3 μm SiO_2 that serves as sacrificial layer. Commercially bought SOI wafers were found to produce an undesired background luminescence in the spectral range of 1.3–1.6 μm, arising from defects created by hydrogen implantation during manufacturing [25, 26]. Therefore, to suppress this background emission we thinned down the Si device layer to 50 nm using hydrofluoric and nitric acids before growing 170 nm of high-purity Si by MBE to achieve a total Si layer thickness of 220 nm. In order to confirm that the regrown wafer exhibits weak background luminescence in the

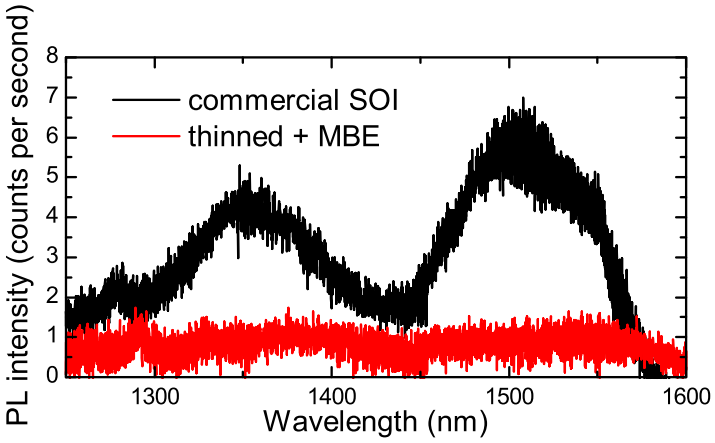

Figure 1. PL intensity at 25 K from an untreated, commercial SOI wafer (black spectrum) and from a commercial wafer, which was thinned and then overgrown with Si using MBE (red spectrum).

spectral region of interest, we compared micro-PL measurements at a temperature of 25 K, from both the delivered and the MBE regrown silicon layers. For optical excitation we used a continuous wave Nd:YAG laser at 532 nm that provided an excitation power of 5 mW focused to a spot size of $\approx 2\,\mu$m ($\approx 160\,\mathrm{kW\,cm^{-2}}$). An imaging monochromator with a spectral resolution of ≈ 0.04 nm was used to disperse the signal onto a multichannel InGaAs detector. A typical PL spectrum recorded at 25 K from an untreated, commercial SOI wafer is presented in figure 1 (black curve) and is compared with the emission from the thinned and overgrown layer (red curve). The results confirm that, by thinning and regrowing, the undesired PL signal is strongly reduced to a level close to the statistical detector noise.

The wafer used for the processing of the active PhC plates was first thinned as described above before being overgrown by 60 nm of Si. Following this, nominally 8 monolayers of Ge were deposited at 410 °C resulting in the self-assembly of Ge islands [27]. The Ge islands were capped by a 110 nm thick layer of Si to obtain a total device layer thickness of 220 nm with the Ge islands located in the center of the Si region. In a final step, a nominally identical layer of Ge islands was deposited on the surface to enable structural characterization using atomic force microscopy. Electron-beam lithography and reactive ion etching were then used to define the plate pattern. The SiO_2 sacrificial layer was removed by diluted hydrofluoric acid in order to obtain free-standing air bridge structures. As described in [22–24], we then removed the plates from the substrate and stacked them to form a 3D PhC using a micromanipulation system installed in the chamber of a scanning electron microscope (SEM).

Figure 2(a) shows a schematic image of the fabricated face-centered tetragonal (FCT) woodpile 3D PhC. The structure has a fourfold basis in the z-direction, consisting of two plates with 11 rods stacked perpendicular to each other, onto which two plates with ten rods are stacked. All plates have a thickness $h = 220$ nm, an in-plane lattice constant of $a = 600$ nm and a rod width $w = 130$ nm. The active plate is sandwiched between ten passive layers below and a variable number of passive layers above. An optical nanocavity is formed by introducing a point defect into the woodpile structure as shown in figure 2(b). The defect connects three rods in such a way that it forms a square region in the x–y-plane [24] producing a defect with an edge length of 1.33 μm. The active plate containing the defect has a single layer of

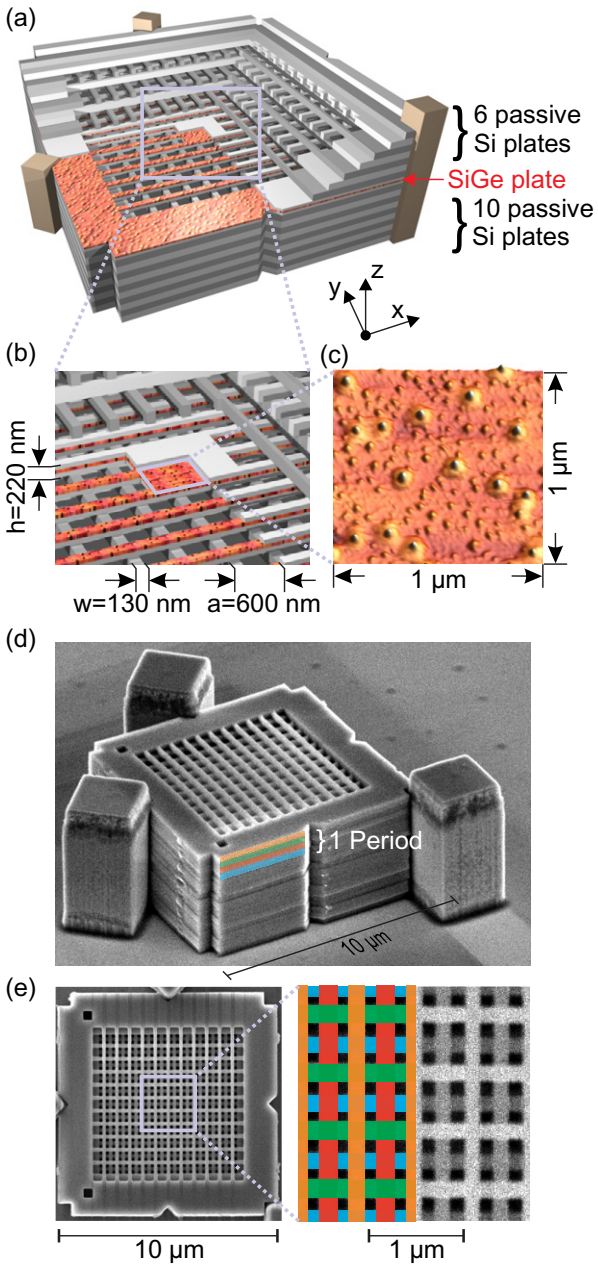

Figure 2. (a) Schematic image of the fabricated 3D FCT woodpile Si PhC with a single layer of Ge islands embedded in the active plate, into which the optical cavity is defined. Upper layers are removed to reveal the cavity structure. (b) Magnified picture of the cavity formed by a square defect connecting three rods. The Ge island layer is centered in the 220 nm thick active plate. (c) $1 \times 1\,\mu m^2$ AFM image showing the Ge islands on top of the active plate. (d) SEM image showing the plates stacked between posts. One period consisting of four plates along the z-direction is highlighted by a colored area on the side of the PhC. (e) Plan view SEM image showing the PhC. A magnification clearly shows the four plates with different rod patterns building the lattice basis along the z-direction. The color coding is adapted from (d).

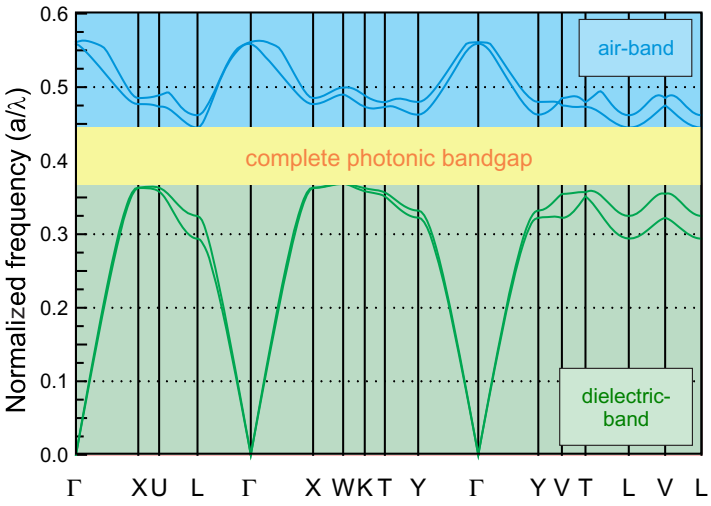

Figure 3. Photonic band diagram showing the lowest four bands as obtained from PWE calculations using the geometric parameters of our FCT woodpile PhC structure. A complete photonic band gap is realized between the air- and the dielectric-band.

self-assembled Ge islands embedded at its midpoint. In figure 2(c), we present an atomic force microscope (AFM) image covering a $1 \times 1\,\mu m^2$ section of an additional layer of optically inactive Ge islands grown on top of the active plate showing a bimodal distribution of 'dome'- and 'pyramid'-shaped nanostructures [27, 28] with a typical density of 20 domes and 100 pyramids per μm^2. Figure 2(d) shows an SEM image of the stacked PhC structure with six upper passive plates stacked onto the defect cavity. The posts permit relative positioning of the plates with an accuracy better than 50 nm [22–24]. A single period of the resulting structure is highlighted by color-shaded areas on the side of the PhC. A higher magnification image, presented in figure 2(e), highlights the precise positioning of the plates relative to each other, and the four plates forming the lattice basis can be clearly distinguished. To emphasize the stacking sequence a fraction of the image is shaded according to the color legend used in figure 2(d).

The photonic band structure of the FCT woodpile PhC is presented in figure 3. It was obtained by performing plane wave expansion (PWE) calculations [29] using the geometric parameters measured for our fabricated structure. These calculations predict a *complete photonic band gap* between the dielectric- and the air-band, covering the normalized frequency range from 0.369 to 0.445 a/λ. With our lattice constant of $a = 600$ nm this corresponds to a band gap ranging from 1348 to 1626 nm with a gap to midgap ratio of 0.187 and a photonic band gap center at 1487 nm.

We have investigated the luminescence from the PhC defect nanocavity using micro-PL at 25 K. Recent work on Ge islands in 2D PhCs has shown that high excitation powers can lead to significant free-carrier absorption [9, 11]. Therefore, we used comparatively low excitation powers of 300 μW focused to a spot size of $\approx 2\,\mu$m ($\approx 10\,kW\,cm^{-2}$) to avoid free-carrier absorption effects. For excitation we used a continuous wave diode pump laser at 660 nm. Figure 4(a) compares typical micro-PL spectra measured at 25 K from the unpatterned sample with embedded Ge islands (gray) with a spectrum from the cavity within the FCT-woodpile PhC with ten (six) passive layers below (above) the active layer (black). The emission from the Ge

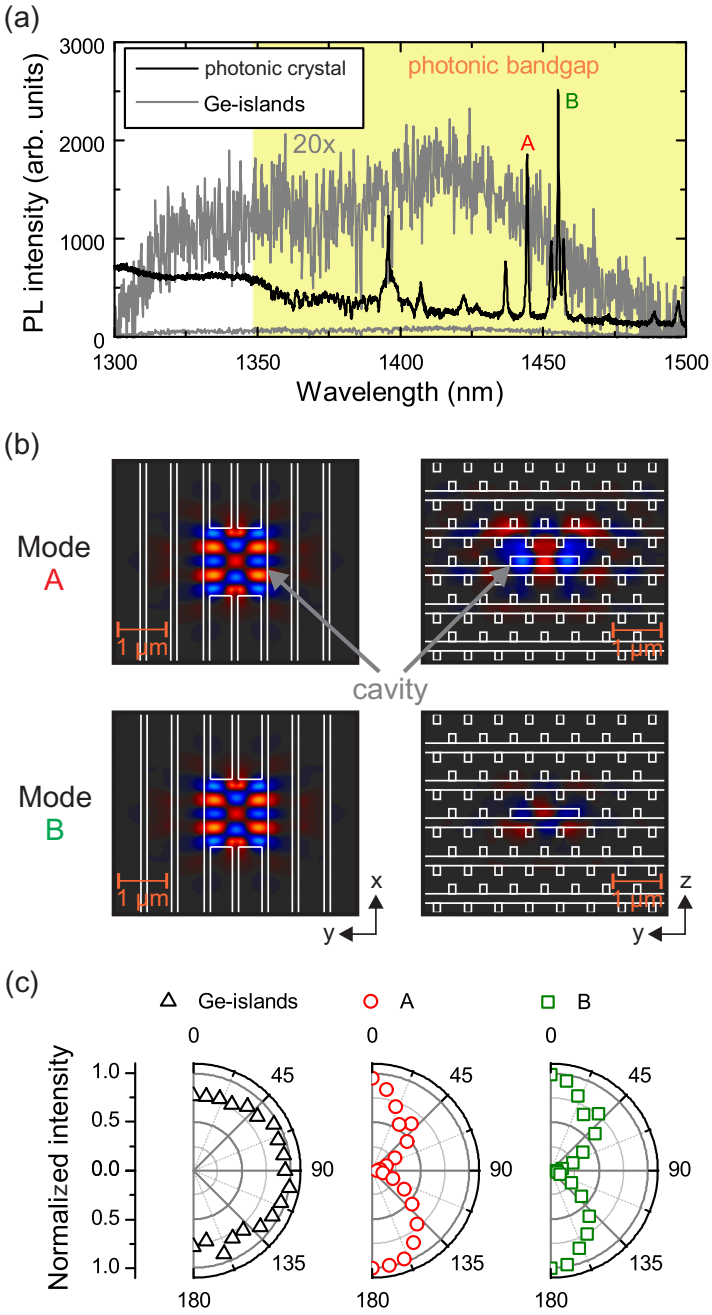

Figure 4. (a) Emission spectrum at 25 K from the unpatterned reference sample with embedded Ge islands (gray) and from the 3D PhC structure (black). The photonic band gap is highlighted by the yellow region. The two strongest modes are labeled A and B. (b) FDTD simulation results showing the electric field distribution of the *y*-component for mode A and mode B in the *x*–*y* and *y*–*z* planes, respectively. (c) Polarization-dependent emission intensity from Ge islands from the reference sample (black triangles), mode A (red circles) and mode B (green rectangles).

islands exhibits a large inhomogeneous broadening arising from size, shape and composition fluctuations [30]. Note the 20× enhanced amplitude of the Ge island reference emission for facilitating a direct comparison. The emission from the Ge islands is quite broad, extending from 1300 to 1500 nm. In comparison, the photonic band gap highlighted by the yellow shaded region on figure 4(a) clearly overlaps the emission from the Ge islands. The black line shows a typical spectrum recorded from the 3D PhC structure. It clearly shows several pronounced resonances inside the photonic band gap and a strong enhancement of the intensity as compared to the results obtained from the unpatterned Ge island sample. The two most prominent peaks are labeled A and B in figure 4(a) and have intensities $30 \pm 2\times$ and $58 \pm 2\times$ stronger than the reference, respectively. We attribute both the peaks to originate from cavity mode emission. Using finite-difference time domain (FDTD) simulations [29], we calculated the y-component of the electric field distribution for both modes. These results are presented in figure 4(b). The left panel shows a cross-sectional view in the x–y-plane through the center of the PhC, and the images on the right side show a cross-sectional cut in the y–z-plane. As can be clearly seen, the electric field is strongly localized to the cavity. While the field profile of both modes shows only a little difference in the x–y-plane, they differ strongly in the y–z-plane. Since the FCT woodpile PhC does not possess inversion symmetry along the z-axis, the field profiles along this direction are non-symmetric as well, in strong contrast with 2D slab PhCs.

Polarization-dependent measurements with linear polarization selectivity in the detection channel clearly show that the Ge islands from the reference sample emit unpolarized light (figure 4(c)). In contrast, peaks A (red circles) and B (green rectangles) are strongly linearly polarized with a degree of polarization $\geqslant 95\%$. The combined observation of sharp spectral features within the photonic band gap and linearly polarized emission provides strong evidence that the observed intense emission arises from Ge islands coupled to the cavity modes [22]. Both cavity modes exhibit quality-factors of $\approx 3650 \pm 90$ for this cavity with six upper plates. We continue by analyzing the evolution of the PL spectrum as a function of the number of upper cladding plates stacked onto the active plate containing the defect on top of ten lower cladding plates. The PL measurements were carried out at 25 K with excitation performed using a continuous wave diode laser at 660 nm with an excitation power of 300 μW, focused to a spot size with a diameter of $\approx 2\,\mu$m. The results for modes A and B are presented in figure 5(a) in a semi-logarithmic representation. The lowermost spectrum was obtained without any upper cladding plates, while the uppermost spectrum was recorded from the same sample after ten passive upper plates had been stacked onto the active plate. The intensities of modes A and B evolve slowly as the first five plates are placed onto the active plate and much more rapidly as further cladding plates are added. A systematic and global redshift of the emission spectrum is observed with increasing the number of top cladding layers, due to the increased localization of the mode inside the high refractive index material (Si) as the reflectivity of the upper cladding plates increases. Most importantly, we observe a continuous reduction of the cavity mode linewidth and thus an increase of the Q-factor upon increasing the number of upper cladding plates. This observation directly reflects the enhanced reflectivity of the omnidirectional photonic band gap and explains the progressive reduction of mode intensity observed as the number of upper cladding plates increases. In the left panel of figure 5(b) we present the Q-factor of modes A (red circles) and B (green squares) as a function of the number of top layers on a semi-logarithmic plot. The Q-factor clearly increases exponentially with the number of upper cladding plates as expected [24]. Both modes show qualitatively the same behavior with an increase of the Q-factor from <1000 for fewer than four top plates to $>10\,000$

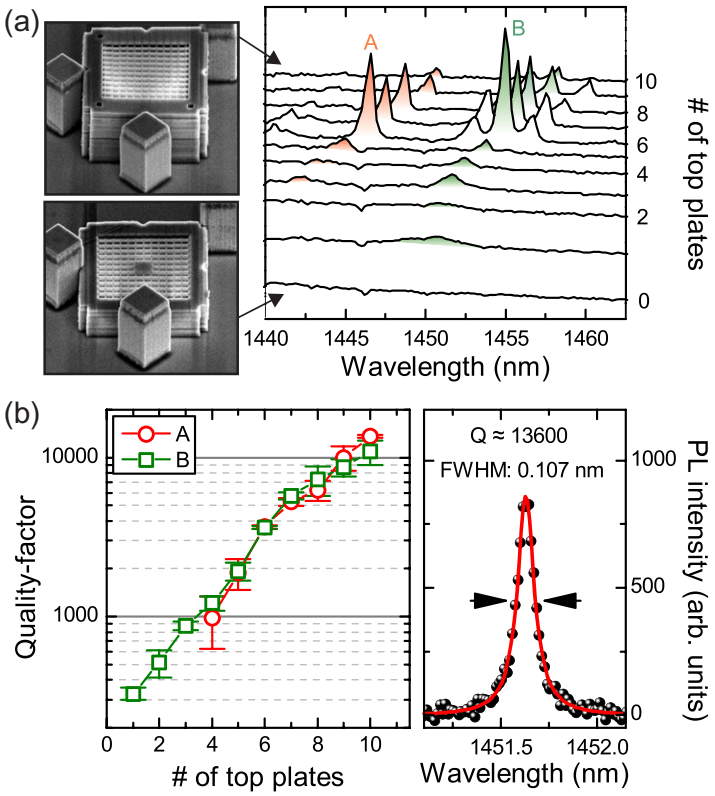

Figure 5. (a) Left: SEM images of the FCT woodpile PhC with and without ten top capping plates. Right: semi-logarithmic waterfall plot showing the evolution of the emission spectrum of modes A and B with increasing the number of top plates. (b) Left: Q-factor of modes A (red circles) and B (green rectangles) as a function of the number of top plates. Right: high-resolution spectrum of mode A for ten top layers with a Lorentzian fit (red line).

for the maximum number of ten cladding plates. A high-resolution spectrum, as recorded from mode A with ten upper cladding layers, is presented on the right panel of figure 5(b). A Lorentzian fit yields a full width at half maximum of 0.107 nm, corresponding to a Q-factor of $\approx$13 600, almost three orders of magnitude higher than any previous report for Si-based 3D PhC cavities [17, 18].

We continue by investigating the pump power dependence of the cavity mode emission from modes A and B after ten passive cladding plates have been placed on the active layer. These measurements provide information about the influence of non-radiative Auger recombination and thus the mechanisms that influence optical efficiency. In figure 6(a), we present typical examples of the emission spectrum in the vicinity of modes A and B for three different excitation powers: 1 μW (yellow), 10 μW (orange) and 100 μW (black). The linewidth of the mode emission is clearly unaffected by the excitation level, indicating that we are pumping below the level at which free-carrier absorption becomes relevant [11]. In figure 6(b), we plot the intensities of modes A (red circles) and B (green squares), extracted from a Lorentzian fit, as a function of excitation power in a double logarithmic representation. For excitation powers between 0.3 and 1.5 μW, we observe an almost linear dependence with exponents $m^*_{\mathrm{A}} = 0.90 \pm 0.04$ and $m^*_{\mathrm{B}} = 0.91 \pm 0.01$. In sharp contrast, starting from 3 μW, both modes

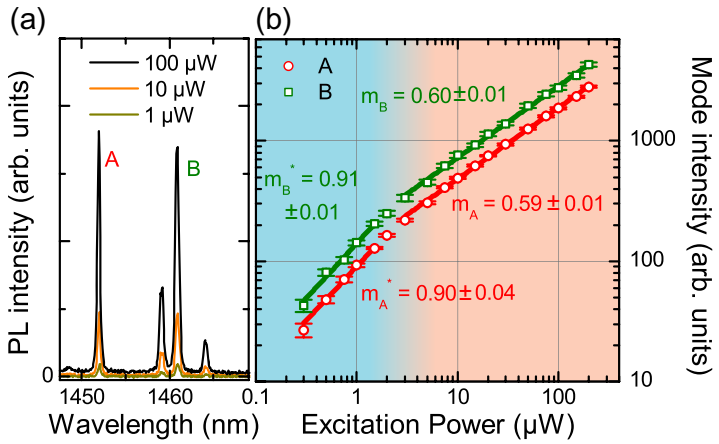

Figure 6. (a) Emission spectrum in the vicinity of modes A and B from the 3D PhC structure with ten passive layers below and on top of the active layer, shown exemplarily for three different excitation powers. (b) Cavity mode intensities of mode A (red circles) and mode B (green squares) as a function of excitation power in a log–log plot. The exponent m is determined by the slope of a linear fit to the data in this plot.

exhibit a clear sublinear dependence of $m_A = 0.59 \pm 0.01$ and $m_B = 0.60 \pm 0.01$, respectively. It has been shown previously that an exponent of 2/3 provides a fingerprint for a system in which radiative decay competes with non-radiative Auger recombination [31]. Therefore, we expect Auger recombination to play a dominant role for excitation powers larger than $3\,\mu$W ($\approx 100\,\mathrm{W\,cm^{-2}}$). We emphasize that we cannot reach the linear regime where radiative decay may dominate the decay dynamics for an identical active plate which consists of a single layer of Ge emitters outside a tailored photonic environment, indicating that the combined optical efficiency is considerably enhanced by the 3D PhC nanocavity. The strongly enhanced emission from the Ge islands inside the PhC cavity allow studies in this low excitation regime, and preliminary time resolved measurements show a threefold shortening of the lifetimes, which may be first evidence for the Purcell effect in these 3D nanocavities.

In summary, we have fabricated a Si 3D FCT woodpile PhC nanocavity with embedded Ge islands. It was assembled layer by layer from lithographically patterned Si-plates using micromanipulation. The MBE grown self-assembled Ge islands were embedded in a single *active* plate into which a defect nanocavity is formed. Using low-temperature micro-PL we could demonstrate radiative coupling to cavity modes with linear polarization. Currently, the maximum cavity Q-factor achieved is $\approx 13\,600$ for a device consisting of 2.5 periods of the 3D Si PhC surrounding the active layer. This value is almost three orders of magnitude higher than has previously been reported for any Si-based 3D PhC.

Acknowledgments

We thank A Laucht for fruitful discussions and H Riedl for expert technical support in sample growth. We acknowledge financial support from the DFG via the cluster of excellence Nanosystems Initiative Munich (NIM), the TUM International Graduate School of Science and

Engineering (IGSSE), the TUM Institute for Advanced Study (IAS), JSPS through the Funding Program for World-Leading Innovative R&D on Science and Technology (FIRST Program) and MEXT of Japan through Project for Developing Innovation.

References

[1] Pavesi L 2004 *Silicon Photonics* (Berlin: Springer)
[2] Jalali B 2007 Teaching silicon new tricks *Nature Photon* **1** 193–5
[3] Iwamoto S, Arakawa Y and Gomyo A 2007 Observation of enhanced photoluminescence from silicon photonic crystal nanocavity at room temperature *Appl. Phys. Lett.* **91** 211104
[4] Fujita M, Tanaka Y and Noda S 2008 Light emission from silicon in photonic crystal nanocavity *IEEE J. Sel. Top. Quantum Electron.* **14** 1090–7
[5] Hauke N, Zabel T, Müller K, Kaniber M, Laucht A, Bougeard D, Abstreiter G, Finley J J and Arakawa Y 2010 Enhanced photoluminescence emission from two-dimensional silicon photonic crystal nanocavities *New J. Phys.* **12** 053005
[6] Li X, Boucaud P, Checoury X, Kermarrec O, Campidelli Y and Bensahel D 2006 Probing photonic crystals on silicon-on-insulator with Ge/Si self-assembled islands as an internal source *J. Appl. Phys.* **99** 023103
[7] Xia J S, Ikegami Y, Shiraki Y, Usami N and Nakata Y 2006 Strong resonant luminescence from Ge quantum dots in photonic crystal microcavity at room temperature *Appl. Phys. Lett.* **89** 201102
[8] Boucaud P *et al* 2008 Germanium-based nanophotonic devices: two-dimensional photonic crystals and cavities *Thin Solid Films* **517** 121–4
[9] El Kurdi M, Checoury X, David S, Ngo T P, Zerounian N, Boucaud P, Kermarrec O, Campidelli Y and Bensahel D 2008 Quality factor of Si-based photonic crystal l3 nanocavities probed with an internal source *Opt. Express* **16** 8780–91
[10] Xia J, Tominaga R, Fukamitsu S, Usami N and Shiraki Y 2009 Generation and wavelength control of resonant luminescence from silicon photonic crystal microcavities with Ge dots *Japan. J. Appl. Phys.* **48** 022102
[11] Hauke N, Lichtmannecker S, Zabel T, Laussy F P, Laucht A, Kaniber M, Bougeard D, Abstreiter G, Finley J J and Arakawa Y 2011 Correlation between emission intensity of self-assembled germanium islands and quality factor of silicon photonic crystal nanocavities *Phys. Rev.* B **84** 085320
[12] Yablonovitch E 1987 Inhibited spontaneous emission in solid-state physics and electronics *Phys. Rev. Lett.* **58** 2059–62
[13] Ho K M, Chan C T and Soukoulis C M 1990 Existence of a photonic gap in periodic dielectric structures *Phys. Rev. Lett.* **65** 3152–5
[14] Lin S, Fleming J G, Hetherington D L, Smith B K, Biswas R, Ho K M, Sigalas M M, Zubrzycki W, Kurtz S R and Bur J 1998 A three-dimensional photonic crystal operating at infrared wavelengths *Nature* **394** 251–3
[15] Blanco A *et al* 2000 Large-scale synthesis of a silicon photonic crystal with a complete three-dimensional bandgap near 1.5 micrometres *Nature* **405** 437–40
[16] Leistikow M D, Mosk A P, Yeganegi E, Huisman S R, Lagendijk A and Vos W L 2011 Inhibited spontaneous emission of quantum dots observed in a 3d photonic band gap *Phys. Rev. Lett.* **107** 193903
[17] Qi M, Lidorikis E, Rakich P T, Johnson S G, Joannopoulos J D, Ippen E P and Smith H I 2004 A three-dimensional optical photonic crystal with designed point defects *Nature* **429** 538–42
[18] Rinne S A, García-Santamaría F and Braun P V 2007 Embedded cavities and waveguides in three-dimensional silicon photonic crystals *Nature Photon* **2** 52–6
[19] Ho K M, Chan C T, Soukoulis C M, Biswas R and Sigalas M 1994 Photonic band-gaps in 3-dimensions—new layer-by-layer periodic structures *Solid State Commun.* **89** 413–16
[20] Özbay E, Abeyta A, Tuttle G, Tringides M, Biswas R, Chan C T, Soukoulis C M and Ho K M 1994 Measurement of a three-dimensional photonic band gap in a crystal structure made of dielectric rods *Phys. Rev.* B **50** 1945–8

[21] Aoki K, Miyazaki H T, Hirayama H, Inoshita K, Baba T, Sakoda K, Shinya N and Aoyagi Y 2003 Microassembly of semiconductor three-dimensional photonic crystals *Nature Mater.* **2** 117–21

[22] Aoki K, Guimard D, Nishioka M, Nomura M, Iwamoto S and Arakawa Y 2008 Coupling of quantum-dot light emission with a three-dimensional photonic-crystal nanocavity *Nature Photon* **2** 688–92

[23] Tandaechanurat A, Ishida S, Aoki K, Guimard D, Nomura M, Iwamoto S and Arakawa Y 2009 Demonstration of high-q (>8600) three-dimensional photonic crystal nanocavity embedding quantum dots *Appl. Phys. Lett.* **94** 171115

[24] Tandaechanurat A, Ishida S, Guimard D, Nomura M, Iwamoto S and Arakawa Y 2011 Lasing oscillation in a three-dimensional photonic crystal nanocavity with a complete bandgap *Nature Photon* **5** 91–4

[25] Lo Savio R, Portalupi S L, Gerace D, Shakoor A, Krauss T F, O'Faolain L, Andreani L C and Galli M 2011 Room-temperature emission at telecom wavelengths from silicon photonic crystal nanocavities *Appl. Phys. Lett.* **98** 201106

[26] Shakoor A, Lo Savio R, Portalupi S L, Gerace D, Andreani L C, Galli M, Krauss T F and O'Faolain L 2011 Enhancement of room temperature sub-bandgap light emission from silicon photonic crystal nanocavity by purcell effect *Physica* B **407** 4027–31

[27] Abstreiter G, Schittenhelm P, Engel C, Silveira E, Zrenner A, Meertens D and Jager W 1996 Growth and characterization of self-assembled Ge-rich islands on Si *Semicond. Sci. Technol.* **11** 1521

[28] Ross F M, Tromp R M and Reuter M C 1999 Transition states between pyramids and domes during Ge/Si island growth *Science* **286** 1931–4

[29] Soft R 2008 Rsoft design group products, http://www.rsoftdesign.com/

[30] Boucaud P, Le Thanh V, Sauvage S, Debarre D, Bouchier D and Lourtioz J M 1998 Photoluminescence of self-assembled Ge dots grown by ultra-high-vacuum chemical vapor deposition *Thin Solid Films* **336** 240–3

[31] Apetz R, Vescan L, Hartmann A, Dieker C and Lüth H 1995 Photoluminescence and electroluminescence of SiGe dots fabricated by island growth *Appl. Phys. Lett.* **66** 445–7